Applied Surface Science Advances 18 (2023) 100502

Contents lists available at ScienceDirect

Applied Surface Science Advances

journal homepage: www.sciencedirect.com/journal/applied-surface-science-advances

Adsorptive removal of Pb^{2+} ions using stable imine linked covalent organic frameworks: A simulated and experimental studies

H. Shanavaz [a], S. Archana [a], M.K. Prashanth [b], K. Yogesh Kumar [a,*], V.S. Anusuya Devi [c], S.B. Benaka Prasad [a], Fahd Alharethy [d], Byong-Hun Jeon [e,*], M.S. Raghu [c,*]

[a] Department of Chemistry, Faculty of Engineering and Technology, Jain University, Bangalore 562112, India
[b] Department of Chemistry, BNM Institute of Technology, Banashankari, Bangalore 560070, India
[c] Department of Chemistry, New Horizon College of Engineering, Outer Ring Road, Bangalore 560103, India
[d] Department of Chemistry, College of Science, King Saud University, Riyadh 11451 Saudi Arabia
[e] Department of Earth Resources and Environmental Engineering, Hanyang University, 222, Wangsimni-ro, Seongdong-gu, Seoul 04763, Republic of Korea

ARTICLE INFO

Keywords:
COF
Solvothermal
Lead removal
Adsorption
Statistical analysis

ABSTRACT

Porous organic frameworks that are bound covalently are eye-catching materials in the current research. The present work describes the solvothermal synthesis of a combination of 3,3′,5,5′-tetramethyl-[1,1′-biphenyl] 4,4′-diamine and benzene-1,3,5-tricarbaldehyde through covalent bonding to generate TBBT-covalent organic framework (TBBT-COF). The structural, morphological, and computational characterizations confirm the formation of COF. TBBT-COF has been used as an adsorbent for the removal of Pb^{2+} ions from aqueous media. The effects of pH, initial metal ion concentration, competing ions, and adsorbent dosage were optimized to attain maximum adsorption of Pb^{2+}. The kinetics follow pseudo-second-order and govern the chemisorption of Pb^{2+} with the imine group of TBBT-COF. The X-ray diffraction (XRD) and X-ray photoelectron spectroscopy (XPS) analyses of TBBT-COF after adsorption of Pb^{2+} support the chemisorption of $Pb^{2+}$with TBBT-COF. The 2D contour and 3D surface response plots were used to assess the specific and comparative effects of the experimental variables. An analysis of variance (ANOVA) of the regression model was used to establish the relevance of the primary influencing variables on the adsorption of Pb^{2+}over TBBT-COF. It was found to remove 99 % of Pb^{2+} in 90 min. The results of the real-sample analysis show the efficient removal of Pb^{2+} even in the presence of other cations. The statistical analysis of the adsorption has been conducted, which indicates the suggested models closely match the experimental data. The high surface area, covalency, and stability of TBBT-COF show its good adsorbent properties.

1. Introduction

Water is an essential natural source that is getting polluted across the globe due to uncontrolled human activities [1,2]. The buildup of heavy metals, dyes, pesticides, insecticides, and pharmaceuticals is the main cause of water pollution [3,4]. Heavy metals are of different types based on their toxicity level. Cu, Fe, Mn, and Co are the essential metals; Zr, Li, Al, and Ba are non-essential metals; Sn and As are less toxic; and Hg, Pb and Cd are highly toxic metals [5,6]. Lead is being used in batteries, tyres, vehicles, pesticides, paints, electroplating, mining, and ceramic industries [7,8]. The high stability of Pb persists in water, accumulates in soil, and then enters the food chain and causes ecological imbalance [9]. The permissible limit of Pb in drinking water is 0.01 mg/L [10,11]. Exposure to Pb causes several health issues among humans, like low fertility, depressive disorder, renal damage, anaemia, peripheral neuropathy, and miscarriage [12–14]. Hence, to reduce these health risks, it is essential to treat the accumulated lead in water.

Many techniques have been found in the literature for the removal of lead, like reverse osmosis, membrane filtration, coagulation, ion-exchange, electrochemical deposition, photocatalysis, and adsorption [15–18]. Many of these methods have their own limitations, like incomplete removal, toxic byproducts, being tedious, not being economical, and requiring high energy [19–22]. Adsorption is a simple surface phenomenon known for its efficiency, simplicity, cost-effectiveness, and speed [23]. A variety of materials have been used as adsorbents, such as clays, aluminosilicate minerals, metal oxides,

* Corresponding authors.
E-mail addresses: yogeshkk3@gmail.com (K.Y. Kumar), bhjeon@hanyang.ac.kr (B.-H. Jeon), dr.msraghu@newhorizonindia.edu (M.S. Raghu).

https://doi.org/10.1016/j.apsadv.2023.100502
Received 1 September 2023; Received in revised form 29 October 2023; Accepted 13 November 2023
Available online 18 November 2023

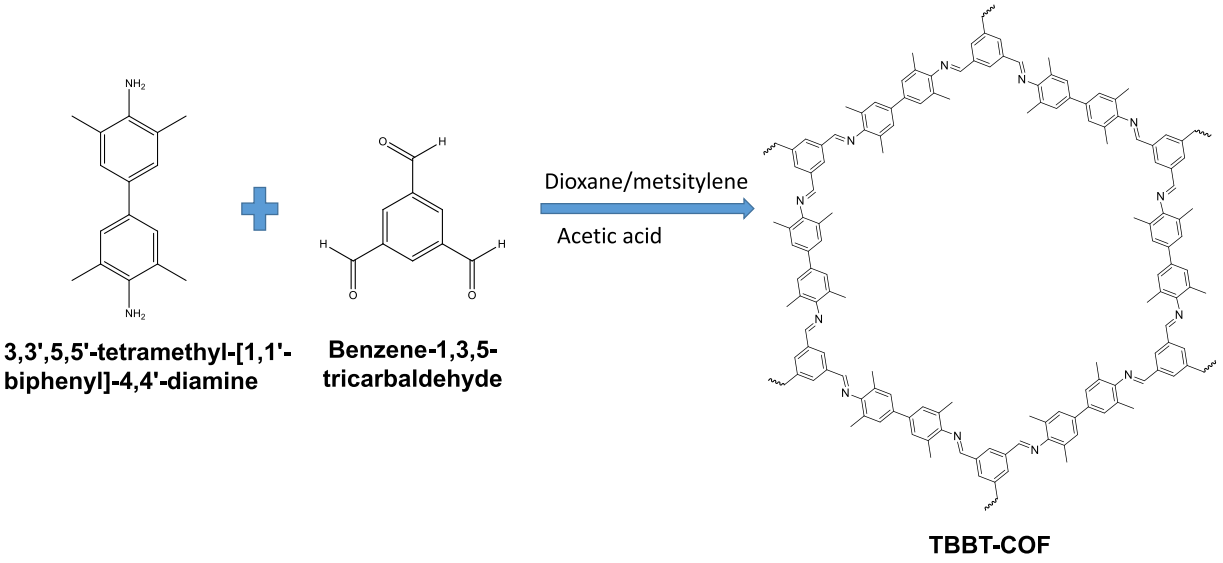

Scheme 1. Synthesis of TBBT-COF.

activated carbon, zeolites, Carbon nanotubes, and graphene-based materials [24–29]. There are several reports on the removal of Pb^{2+} ions using carbon based materials from aqueous solution [30–34]. All these methods exhibit major limitations like lower surface area, non crystallinity, low porosity, low stability, and difficult synthetic strategies [35, 36]. Hence, the development of materials with high porosity, stability, and enhanced surface area with suitable adsorption sites is in high demand.

Covalent organic frameworks (COFs) are a class of metal-free polymeric materials with good stability due to π-π interactions. COFs exhibit high surface area, highly ordered arrangement, and sufficient porosity [37–39]. The predesigned structure of COFs is an additional advantage and consists of light metals like carbon, nitrogen and oxygen moieties. In addition, COFs consist of continuous building blocks that are interweaved through strong covalent bonds [40,41]. The characteristics of COFs are attractive and hence find applications in energy storage, photocatalysis, adsorption, catalysis, sensors, optoelectronic devices, and drug delivery [42–44].

The dimensionality, porosity, and versatile structures of COFs mainly depend on synthetic strategies. COFs have been widely synthesized using solvothermal, microwave, ionothermal, sonochemical, electron beam-induced, and mechanochemical methods [45–47]. Most of these methods have their own drawbacks, like impurities in the end product, the use of UV light, which is not economical, the use of an ultrasonicator, low productivity, and reactor erosion. The solvothermal method using pyrex tubes for the synthesis of COFs is well known for the generation of stable crystals.

The authors in the present work describe the solvothermal method in a pyrex tube using 3,3′,5,5′-tetramethyl-[1,1′-biphenyl] 4,4′-diamine (TBD), and benzene-1,3,5-tricarbaldehyde (BTC) to synthesize TBBT-COF through imine linkage. Certainly, the use of imine-linked TBBT-COF for the removal of Pb^{2+} ions is indeed a relatively novel and innovative concept. Heavy metal pollution, with a particular focus on lead (Pb^{2+}), stands as a formidable environmental concern of our times. This research makes a significant contribution to the collective endeavour of discovering efficient and sustainable methods for remediation. By targeting the removal of Pb^{2+} ions using imine-linked TBBT-COF, the work not only acknowledges the gravity of the issue but also propels us toward a cleaner and more sustainable environmental future. The integration of both simulated (theoretical) and experimental (real-world) studies in this research is a groundbreaking and holistic methodology. This dual approach not only bolsters the credibility of the findings but also enriches the study with a well-rounded perspective, ensuring a thorough understanding of the removal process for Pb^{2+} ions using imine-linked TBBT-COF. A statistical analysis of adsorption has been conducted using various mathematical models. To comprehend the capability of adsorbing target metal ions combined with competing cations, real sample analysis has been assessed. This research opens up the possibility of using different COFs to remove pollutants from water through adsorptive means.

2. Experimental

2.1. Materials

Chemicals required for all the expermentaions were procurreed from Merck India Pvt. Ltd. All the chemicals are of AR grade and double distilled water was used through out unless its mentioned. All the solvents and acids mentioned were used directly without any further purification. 3,3′,5,5′-tetramethyl-[1,1′-biphenyl] 4,4′-diamine ($C_{16}H_{21}ClN_2$), Benzene-1,3,5-tricarbaldehyde ($C_9H_6O_3$), Acetic acid (CH_3COOH), N,N-dimethyllformamide (C_3H_7NO), tetrahydrofuran (C_4H_8O) were used for the synthesis of –TBBT-COF. Sodium hydroxide (NaOH), Hydrochloric acid (HCl) and Lead Nitrate ($Pb(NO_3)_2$) were used for adsorption experiments.

2.2. Synthesis of TBBT-COF

1 mmol (240 mg) of 3,3′,5,5′-tetramethyl-[1,1′-biphenyl] 4,4′-diamine (TBD), 2 mmol (320 mg) of Benzene-1,3,5-tricarbaldehyde (BTC), and the appropriate amount of mesitylene and acetic acid solution were taken in a 10 mL test tube. The solution was transferred to a pyrex tube after being ultrasonically treated for 25 min. The tube underwent three cycles of freeze-pump-thaw to remove air bubbles before being placed in a liquid N_2 bath. Next, we sealed the tube and heated it to 120 °C for 24 h. A TBBT-COF was prepared (Scheme 1) by collecting the precipitate by centrifugation, washing it with N,N-dimethyllformamide (DMF) and tetrahydrofuran (THF), and then dried in 4 h at 120 °C. The reaction yield was found to be 87 %.

2.3. Instrumentation

In order to obtain the X-ray diffraction (XRD) patterns, a Bruker D2 Phaser XRD equipment was used. Scanning electron microscopy (JEOL

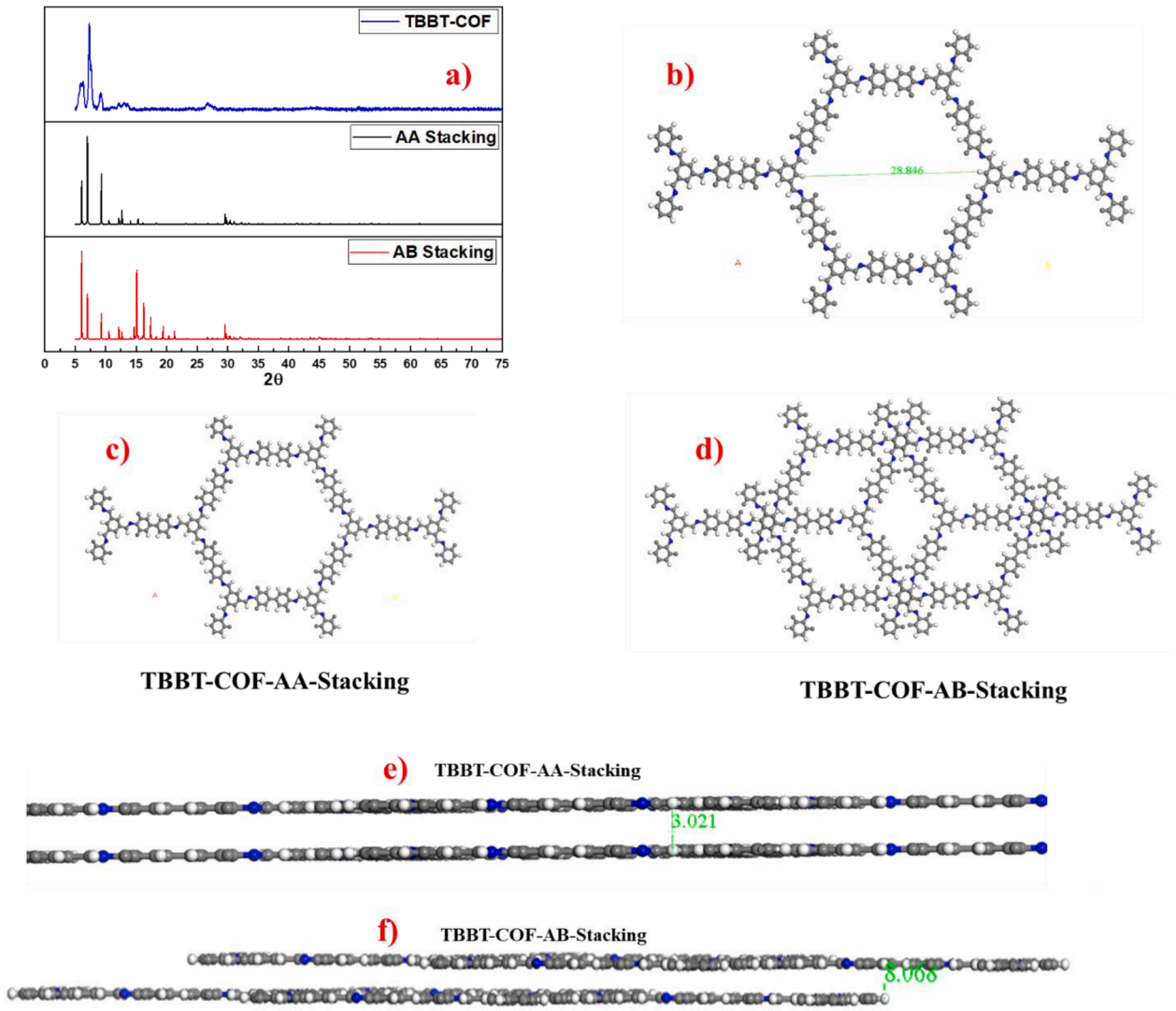

Fig. 1. a) Experimental and simulated XRD curves TBBT-COF, b) Simulated structure of TBBT- COF, c) TBBT-COF AA stacking, d) TBBT-COF AB stacking, e) TBBT-COF AA stacking interlayer spacing and f) TBBT-COF AB stacking interlayer spacing.

JSM 840) with energy dispersive spectroscopy (EDS) was used to investigate the surface morphology (SEM). The images from the TEM were captured with a Philips CM-200 camera. Using an ASAP 2010 Micrometrics instrument calibrated with the Brunauer-Emmett-Teller (BET) method, the TBBT-COF's BET surface area, total pore volume, and average pore size were determined. KRATOS-AXIS ULTRA DLD with Al-Kα radiation (1486.6 eV) was used for X-ray photoelectron spectroscopy (XPS) analysis.

2.4. Sensitivity analysis

The competitive adsorption from a mixture containing 1 mM of K^+, Na^+, Mg^{2+}, Co^{2+}, Cu^{2+}, Cr^{3+}, Cd^{2+}, Hg^{2+}, and Pb^{2+} ions over pH values of 2 and 6 has been evaluated. To these solutions (10 mL), 0.01 g TBBT-COF was added and allowed to attain equilibrium for 1 h. pH of the solution was adjusted using 0.1 M HCl/NaOH. Further adsorption studies were conducted for the highest selective metal ions.

2.5. Batch adsorption experiments

The adsorption efficiency of TBBT-COF was examined using the batch method. Batch experiments were conducted in 100 mL conical flasks by adding 25 mL of Pb^{2+} at concentrations of 100, 200, 300, and 400 ppm. Time was varied from 10 to 90 min, pH (1.0 to 8.0), and Pb^{2+} concentration (100 to 400 ppm) were optimised in three steps. The DPASV method was used with the Electrochemical Workstation (CHI 660D) to assess the metal ion concentration. The evaluation was carried out in a three-electrode electrochemical cell consisting of a counter electrode (platinum wire), a reference electrode (saturated calomel), and a working electrode (glassy carbon, $\varnothing = 3$ mm). After 90 min of adsorption, the solutions were filtered and evaluated for regeneration studies. Eqs. (1) and (2) have been used to calculate the amount of Pb^{2+} that remained during the adsorption process and the removal percentage, respectively.

$$q_e = \frac{(C_i - C_e)V}{w} \tag{1}$$

$$Removal\% = \frac{C_i - C_e}{C_i} \times 100 \tag{2}$$

q_e is the concentration of the adsorbent phase at equilibrium (mg/g adsorbent),

C_i initial concentrations (mg/L)

C_e final (equilibrium) concentrations (mg/L),

V solution volume (L)

w sorbent weight (g) [48].

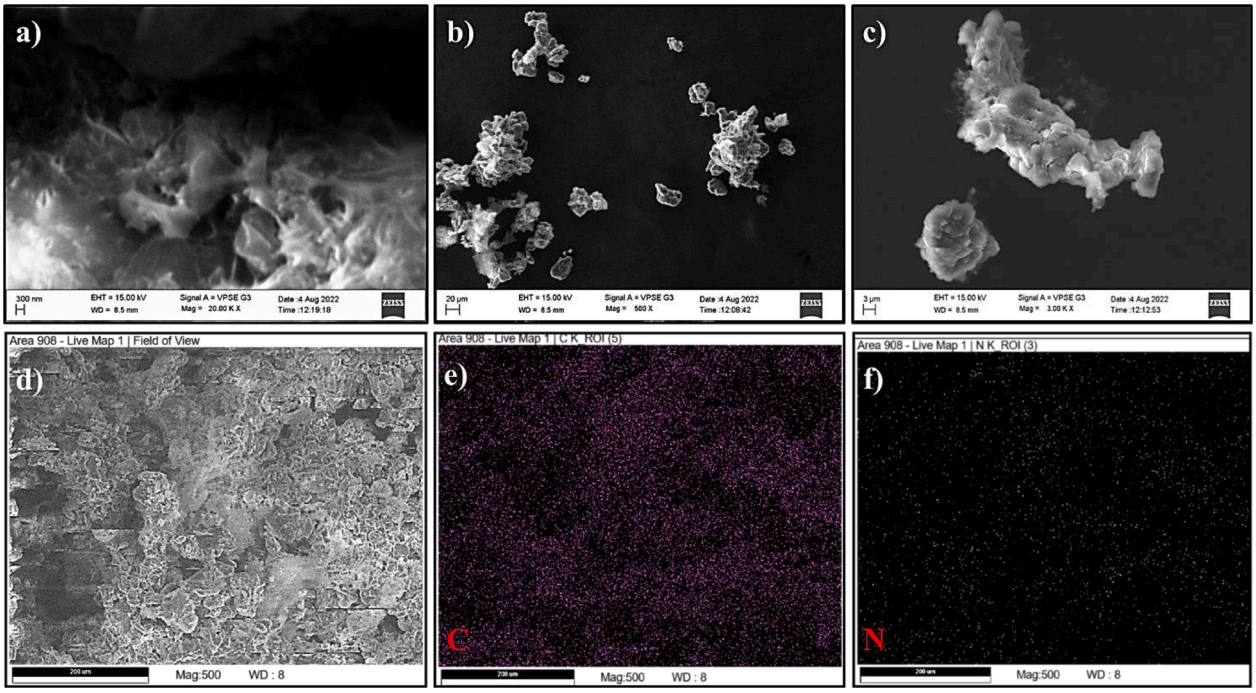

Fig. 2. TBBT-COF a-c) SEM monograph, d) EDS mapping e) C and f) N.

2.6. Statistical analysis

2.6.1. Box-Behnken design experimental design

Using RSM-based Box-Behnken design (BBD), the model parameters corresponding to the highest removal efficiency are evaluated. The RSM-BBD is a strong tool that is frequently used to optimise the key operational variables that influence the adsorption process. Additionally, the statistical analysis sheds light on how the specified process factors interact with one another. In RSM, the response parameter and the control parameter are related through a model equation. Utilizing Design-Expert software (12 versions), Pb^{2+} adsorption onto TBBT-COF from aqueous solutions was modelled and optimized.

In this analysis, time (A), pH (B), and Pb^{2+} concentration (C) were used as controlling variables to figure out how well TBBT-COF removed the Pb^{2+}. The three variables were set up in a three-level BBD with the codes 1, 0, and +1. The chosen variables were run 15 times. The concentrations and variables applied in this study, which is followed by the experiments, are listed in Table S1. Coefficients of determination, analysis of variance, and analysis graphs were used to analyse the obtained results. These were further fitted to the following three-variable quadratic polynomial equation.

$$Y(\%) = \beta_0 + \sum_{i=1}^{3} \beta_i X_i + \sum_{i=1}^{3} \beta_{ii} X_i^2 + \sum_{i<j} \beta_{ij} X_i X_j \quad (3)$$

where Y represents the Pb^{2+}adsorption efficiency;

X_i is the considered variables;

β_0, β_i, β_{ii} and β_{ij} are the intercept, quadratic, linear, and interaction effects, respectively.

2.6.2. Statistical error analysis

The nonlinear regression analysis on equilibrium and kinetic models was performed using experimentally obtained results. Experimental data were calculated using Microsoft Excel. Using the following statistical parameters, the goodness of fit was analysed: SSE, APE, χ2, RMSE, HYBRID, ARE, SAE, AIC, NSD, MPSD and AICc. The mathematical formulations for statistical parameters are shown in Table S2 (Equations 4–12) [49].

2.7. Study of kinetics and isotherm

Four kinetic models were applied to analyse the adsorption behaviour of TBBT-COF.

(i) Lagergren pseudo-first-order equation depending on solid capacity [50]
(ii) Ho and Mckay 'pseudo-second-order reaction on the solid phase sorption model [51]
(iii) intra-particle diffusion [52]
(iv) Elovich kinetic model [53]

The equilibrium isotherm of adsorption was calculated using three isothermal models.

(i) Langmuir isotherm[54]
(ii) Freundlich isotherm[55]
(iii) Dubinin-Radushkevich isotherm [56].

3. Results and discussion

3.1. Material characterization

The experimental XRD patterns of TBBT-COF and the simulated data are in good agreement, as seen in Fig. 1a. The peaks positioned at 2θ-6.32, 7.34, 9.36, 13.18 and 26.76°, which are perfectly indexed to the (100), (110), (200), (220), and (001) diffractions, respectively. Materials Studio version 7.0 was used for research into lattice simulation and structural optimization. TBBT-COF is found to have the space group P6. The Pawley refinement afforded the hexagonal unit cell with parameters of $a = b = 29.089$, $c = 3.02$ and the phase angle $\alpha = \beta = 90^0, \gamma = 120^\circ$ for TBBT-COF. The TBBT-COF pores are 28.84 A^o in width (Fig. 1b), which also confirms the formation of a hexagonal lattice, and the results are in agreement with the BET explained below. The positions of peaks and intensities of the simulated AA stacking modes (Fig. 1c) were in agreement with those of the experimental XRD patterns. The experimental results are indicative of the structural arrangement of the prepared sample, which is inconsistent with the staggered AB stacking modes

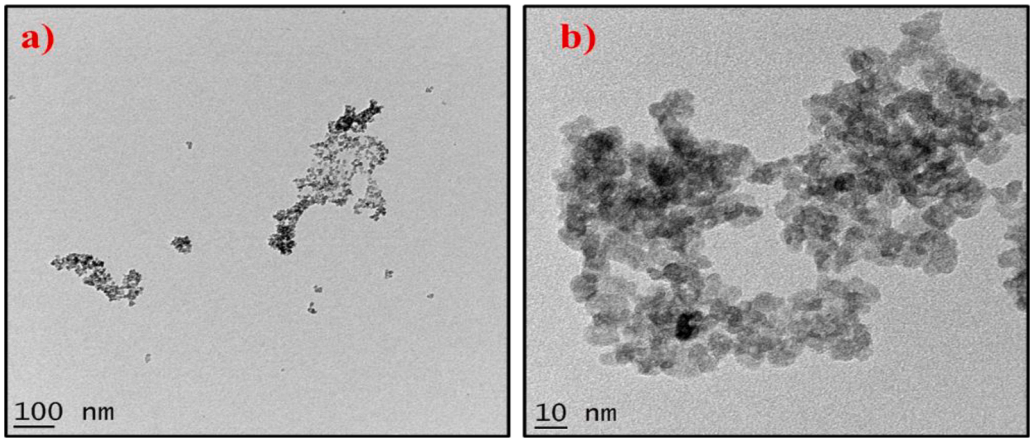

Fig. 3. TEM images of TBBT-COF.

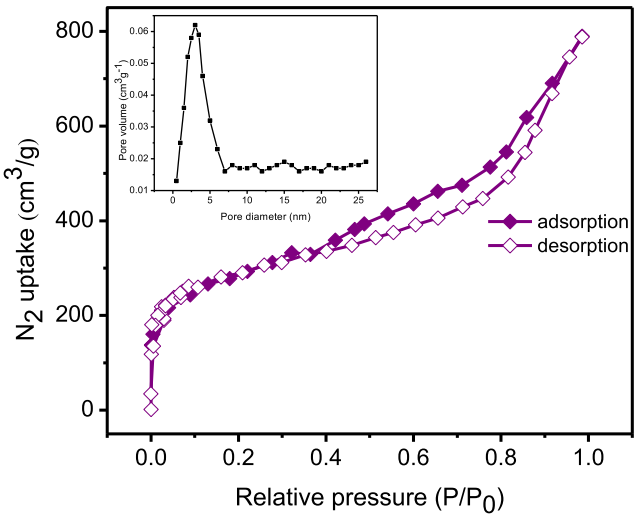

Fig. 4. N_2 adsorption curve (inset: Pore size).

(Fig. 1d). The interlayer distance for AA and AB stacking was found to be 3.02 A° and 8.06 A° respectively (Figs. 1e and 1f). The distance between AA layers at 26.76, where the (001) diffraction peaks occur, is consistent with the π-π stacking distance between vertically stacked aromatic layers.

Adsorbent surface shape and composition were investigated using scanning electron microscopy (SEM) combined EDS analyses. Loosely packed flakes of a small spheroidal size can be seen in Figs. 2a–c. Although an average diameter of 100 nm was achieved, its shape resembled that of irregularly packed flakes and was not clearly defined. Because of the formation of frameworks, TBBT-COF has a rough surface. Due to the undefined shape and crystallinity, of TBBT-COF through SEM analysis, samples were further investigated using transmission electron microscopy. No other impurities besides C and N have been detected by EDS mapping, and the presence of these elements is homogeneous throughout the adsorbent (Figs. 2d–f). TEM scans, as shown in Fig. 3, revealed an aggregate of flakes with a rather uniform size and a roughly spherical morphology.

The fact that its nitrogen adsorption isotherm at 77 K fits the type IV isotherm curve (Fig. 4) shows that TBBT-COF is a mesoporous material. The voids created by the loose accumulation of particles caused the nitrogen absorption to increase dramatically with a hysteresis loop when P/P0 > 0.9. Surface areas calculated using the Brunauer-Emmett-Teller (BET) method were found to be 842 m^2/g. Alternatively, a value of 28.37 A° was determined for the material's porosity by fitting the adsorption curve with generalized function theory (NLDFT), as shown in (*inset* Fig. 4). Adsorption is considerably aided by the TBBT-COF due to its large specific surface area and narrow pore size distribution, as shown above and as indicated by the simulated calculations.The broad peak observed from 2800 to 3100 cm^{-1} in the FTIR spectrum of TBBT-COF (Fig. S1) can also be related to the physically adsorbed water molecules and the unreacted amine groups on the margins of the TBBT-COF sheets. The peaks appearing in the area of 1449– 1601 cm^{-1} related to the formation new imine linkages. The peaks at 1395 and 1205 cm^{-1} can be assigned to aromatic C–N and C–C ring stretching vibration, respectively. The peak at 782 cm^{-1} corresponds to the out-of-plane bending vibration of aromatic C–H. Consequently, these results clearly confirmed the successful formation of a polymer network of TBBT-COF.

3.2. Adsorption study of Pb^{2+} onto TBBT-COF

3.2.1. Selectivity of metal ions

Targeted ions do not often exist alone in real-world applications but instead coexist with competing metal ions. The heavy metal adsorption from various sources into adsorbents is caused by the interaction of the solute with the surface functionality through electrostatic, weak Van der Waals forces of attraction, the formation of complexes, and even hydrogen bonding. Additionally, it was observed that the adsorbent operates differently in the adsorption of a multi-metal ion solution even when the pH conditions are the same. The selectivity of heavy metal ion adsorption is known to be significantly influenced by the initial pH of the metal ion mixture. This is so because pH has an impact on both the surface charge of the adsorbents and the chemical structure of metal ions in solution. Consequently, it is crucial to investigate how these types of parameters affect the sensitivity of the adsorption mechanism. Fig. 5a shows the metal ion adsorption selectivity following TBBT-COF adsorption experiments. When adsorption selectivities for TBBT-COF were taken into account, the material recorded 99 % adsorption capability towards Pb^{2+} ions at pH 6. The type of chelation effect, the metal ion's hardness or softness, the oxidation state of the metal ion, the ligand, the ionic potential, and the ionic size of the metal ions are often factors that affect the unique molar selectivity of ligands [57,58]. Therefore, it was noted that, under similar pH conditions, the adsorbent will function differently in the adsorption of a multi-metal ion solution. Particularly, the capacity for complexation is a major cause of adsorption. According to Table 1, which lists the ionic size and electronegativity of the several metal ions tested in this work, Pb^{2+} has the highest ionic radius (1.19) and electronegativity (2.33) [59–62]. In addition to the ionic radius, the imine group in the TBBT-COF has the ability to chelate, which accounts for the 100 % selectivity towards Pb^{2+}. In the preferred molar selectivity at pH 2, ionic radius also plays a small but

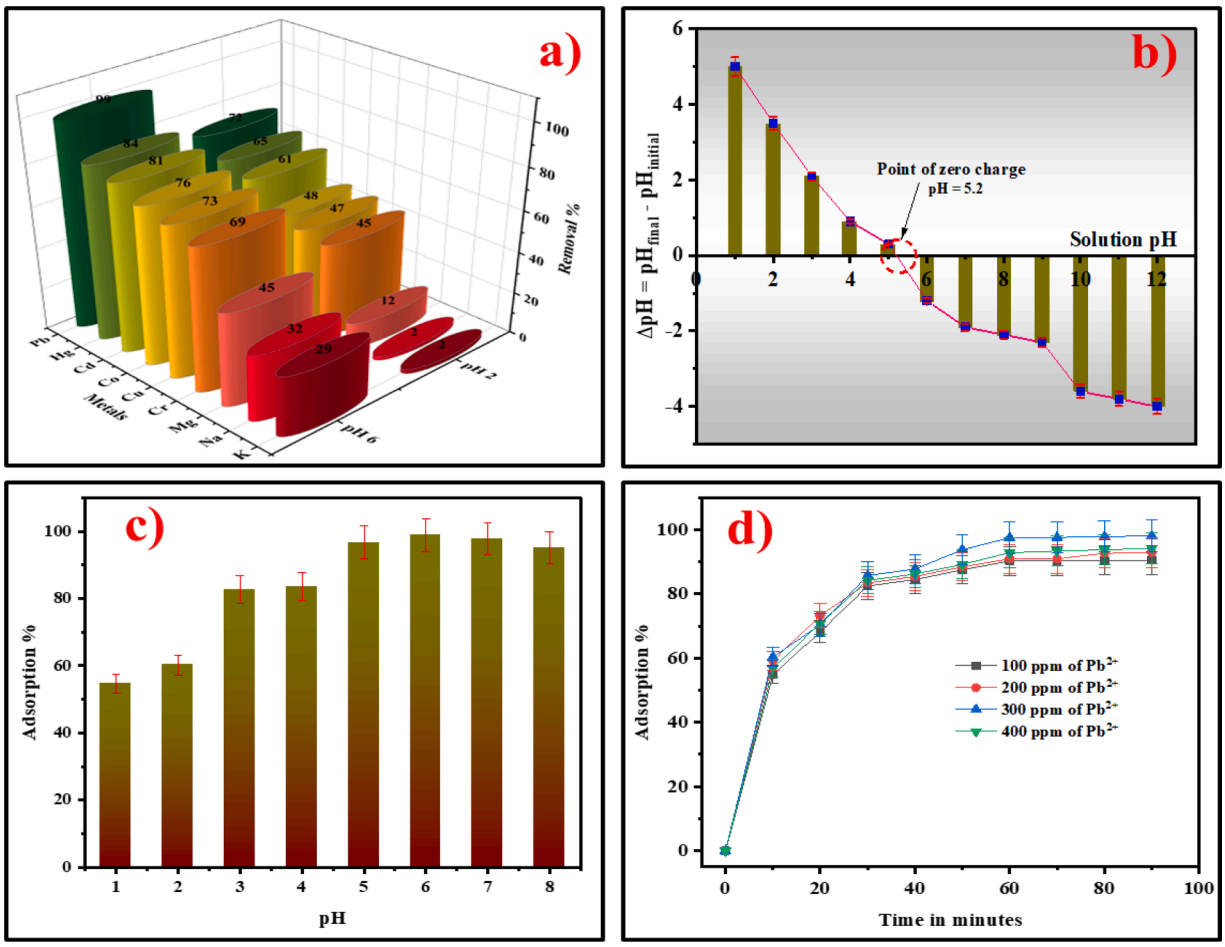

Fig. 5. a) Selectivity of COF towards various metal ions (pH=2&6, Concentration=200 ppm, Dosage=20 g/L), b) Point of zero charge, c) Effect of pH (pH=1–8, Concentration=200 ppm, Dosage=20 g/L) and d) Effect of initial adsorbent concentration (pH=6, Concentration=100–400 ppm, Dosage=20 g/L).

Table 1
Physico-chemical properties of the various metal ions.

Metal ion	Hard / Soft / Intermediate acids	Ionic radius (Å)	Electronegativity
Pb^{2+}	Intermediate	1.19	2.33
Hg^{+}	Soft	1.02	2.00
Cd^{2+}	Soft	0.97	1.69
Co^{2+}	Intermediate	0.74	1.88
Cu^{2+}	Soft	0.73	1.99
Cr^{2+}	Hard	0.52	1.66
Mg^{2+}	Hard	0.72	1.31
Na^{+}	Hard	1.38	0.93
K^{+}	Hard	1.02	0.82

significant role. Pb^{2+} has a higher positive character than all other ions because of its higher ionic radius. At pH 2, Pb^{2+}may compete with H^{+}during adsorption and can readily accept the pair of electrons present in TBBT-COF. This may possible due to the reduced adsorption of Pb^{2+}ions at pH 2.

3.2.2. *Point of zero charge (PZC)*

The pH at which there is no net charge density on the adsorbent's surface is known as PZC. The graph of $\Delta pH = pH_{Final}\text{-}pH_{Initial}$ is shown in Fig. 5b. The PZC value of TBBT-COF is 5.2. Since all adsorbent solution values equilibrate at pH-5.2, the adsorbent surface has a net positive charge below and a net negative charge above this point.

3.2.3. *Effect of pH*

Batch tests were performed at various pH levels (from 1 to 8) to evaluate the impact of pH on the sorption of Pb^{2+}. At low pH values, Fig. 5c demonstrates a considerable reduction in the lead removal percentage; maximum removal was seen between pH values of 4 and 6, while slightly lower removal was seen at higher pH levels. There may be less adsorption at lower pH levels due to hydrogen ions' competition with metal ions for exchangeable cations on the surface of the absorbent. Lead precipitates as hydroxides at higher pHs, which slows down the rate of adsorption. Another explanation for this is that the pH adjustment caused a rise in the concentration of Na^{+} in the solution, which competes with the Pb^{2+} that is still there [63].

3.2.4. *Effect of metal dosage*

Adsorption mechanisms are significantly influenced by the interface between the metal ion and the adsorbent. To investigate how the adsorbate dosage impacts the adsorption behaviour, various Pb^{2+} concentrations were utilised. Due to the increasing number of accessible binding sites, as given in Fig. 5d, the Pb^{2+}removal percentage increased (from 100 to 300 ppm) with the adsorbent dose starting at 20 g/L. Due to the restricted number of liquid phase binding sites at high concentrations (400 ppm), the removal efficiency remains nearly constant. Once the surface has been blocked for 60 to 70 min, the metal ions are not able to enter the interior pores. These results demonstrate that adsorption depends on binding sites. Also, the relationship between the amount adsorbed and the amount of adsorbent is inverse [64].

Table 2
Kinetic parameters for the adsorption of Pb^{2+} on TBBT-COF (pH=6, Concentration=200 ppm, Dosage=20 g/L).

Model		Pb^{2+} on TBBT-COF			
		100	200	300	400
Pseudo-first-order	$q_{e\ (cal)}$ mg/g	12.88	14.54	17.74	19.44
	k_1 min^{-1}	0.047	0.044	0.040	0.034
	R^2	0.88	0.93	0.93	0.92
	$q_{e\ (exp)}$ mg/g	311.71	632.72	971.02	1283.30
Pseudo-second-order	$q_{e\ (cal)}$ mg/g	373.13	699.30	1092.70	1436.53
	K_2 min^{-1}	0.052	0.093	0.076	0.071
	R^2	0.99	0.99	0.99	0.99
	$q_{e\ (exp)}$ mg/g	311.73	632.72	971.01	1283.32
Elovich kinetics	Alpha	5.15	122.73	137.57	737.78
	Beta	69.18	113.23	181.74	245.82
	R^2	0.94	0.99	0.97	0.98
Intra particle diffusion	I mg/g	87.84	277.32	390.35	481.43
	K_i mg/g min	24.01	39.37	62.43	84.3
	R^2	0.94	0.99	0.97	0.98

3.3. Adsorption kinetics, isotherms and thermodynamics

The pseudo-first-order, pseudo-second-order, Elovich, and intra-particular diffusion kinetic models were used to fit the experimental data in order to study the adsorption behaviour of Pb^{2+} on the TBBT-COF. Table 2 contains a list of the kinetic constants, and Fig. 6a–d show a comparison of the results and fitting lines. The experimental results fit the pseudo-second-order model satisfactorily (R^2 = 0.99), better than the pseudo-first-order (R^2 = 0.91) and Elovich models (R^2 = 0.91). Additionally, the estimated Qe, cal was found to be close to the empirically determined Qe,exp, demonstrating the suitability of the pseudo-second-order to forecast the experimental data. Thus, it is demonstrated that Pb^{2+} adsorption differed from the pseudo-first-order kinetic model. The pseudo-first-order model is appropriate, with the exception of the area where the adsorption happens rather quickly. The intensity of the ionic interaction between TBBT-COF and Pb^{2+} is high as Pb^{2+} has high electronegativity and ionic radius. as demonstrated by the fitness of the pseudo-second-order model, which is in agreement with the effects of pH and adsorbent dosage. The linear graph illustrates that the adsorption mechanism under investigation is governed by the chemisorption principle. TBBT-COF contains a polar imine group. This group is in charge of the cation exchange capability with Pb^{2+} and is capable of chemical bonding. The mechanism for the sorption of divalent lead ions onto TBBT-COF is explained below [65].

The above mentioned mechanism may include valency forces

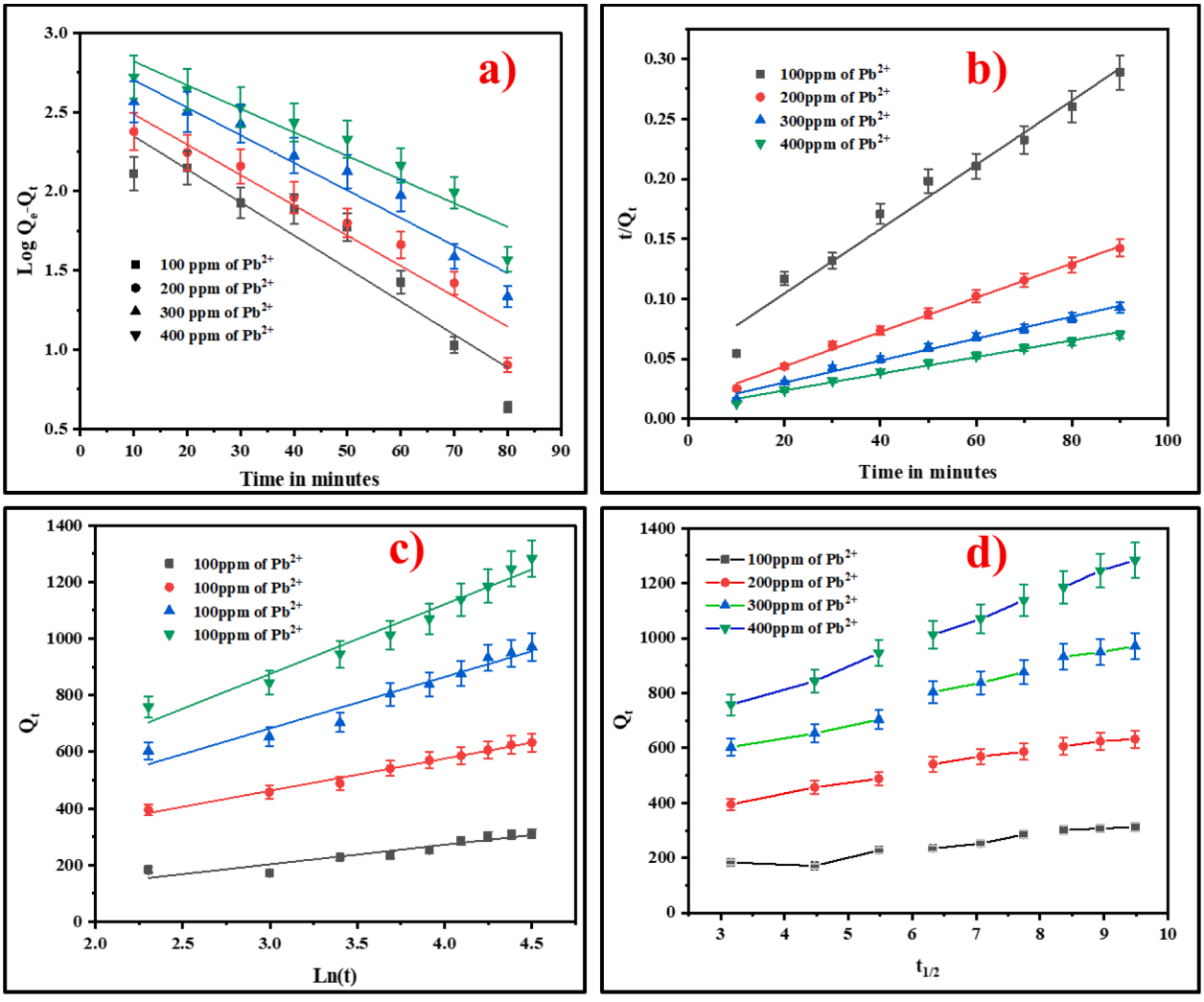

Fig. 6. a) Pseudo-first-order model, b) Pseudo-second-order model, c) Elovich and d) Intra particular diffusion for the adsorption (pH=6, Concentration=200 ppm, Dosage=20 g/L).

Table 3
Isothermal parameters for the adsorption of Pb^{2+} on TBBT-COF (pH=7, Concentration=200 ppm, Dosage=20 g/L).

Model		Pb^{2+}
Langmuir isotherm	q_e mg/g	601.6
	k_L L/mg	0.52
	R^2	0.99
Freundlich isotherm	n	0.63
	K_f (mg /g)(L/mg)$^{\frac{1}{n}}$	18.47
	R^2	0.94
DR Isotherm	E	522.2
	q_m mg/g	1863.12
	R^2	0.96

through the sharing or covalent exchange of electrons between the adsorbate and adsorbent. The Pb^{2+}ions and the significant number of C—N groups that are present on the adsorbent surface may interact in intermediate-soft interactions, which could explain the high adsorption capacity. Additionally, cation interactions between Pb^{2+} ions and the double bonds of the adsorbent can be thought of as another factor impacting the adsorption of Pb^{2+} ions. Furthermore, the adsorption of Pb^{2+}ions can be significantly influenced by the electrostatic attraction between the mesoporus ring and Pb^{2+}ions. Because of the reversible interaction between the Pb^{2+} ions and the synthesised adsorbent, which is evident from the results of the recovery studies, it is less likely that they will form strong covalent bonds with one another [66].

The rate-limiting effect of diffusion is thought to be much more frequent in TBBT-COF adsorption, as shown by the R^2 values of the Elovich model being relatively high in all concentrations. The mass transfer paths that occur during the adsorption were clarified using the intraparticle diffusion model, and the fitting parameters are provided in Table 2. The three successive steps of the Pb^{2+} adsorption process onto TBBT-COF are depicted in Fig. 6d. The first one describes the process of boundary layer diffusion or Pb^{2+}adsorption on TBBT-COF exterior surface sites. Intra-particle diffusion is a rate-controlled process in the second stage. The equilibrium condition represented by the final step shows how the rate of intraparticle diffusion was slowed down by an overly low concentration of Pb^{2+} molecules [67]. These results were further reinforced by the fact that the rate constant (K_{int}) values for Pb^{2+} decreased from the first to the last stage ($K_{int}1 > K_{int}2 > K_{int}3$).

In order to understand how Pb^{2+} is distributed at the liquid/TBBT-COF contact, equilibrium adsorption isotherms are crucial. The ideal experimental conditions were used to conduct the equilibrium adsorption study. The Langmuir, Freundlich, and DR isothermal models were used to simulate the Pb^{2+} adsorption equilibrium process on the TBBT-COF surface. Table 3 contains the formulas for the Langmuir, Freundlich, and DR models, and Fig. 7a–c shows their fitting plots for Pb^{2+} adsorption on the TBBT-COF surface. As observed from the R^2 values in Table 3, the Langmuir model ($R^2 = 0.99$) adjusted for experimental data (Qm.exp) suits well and is found to be better than the Freundlich model

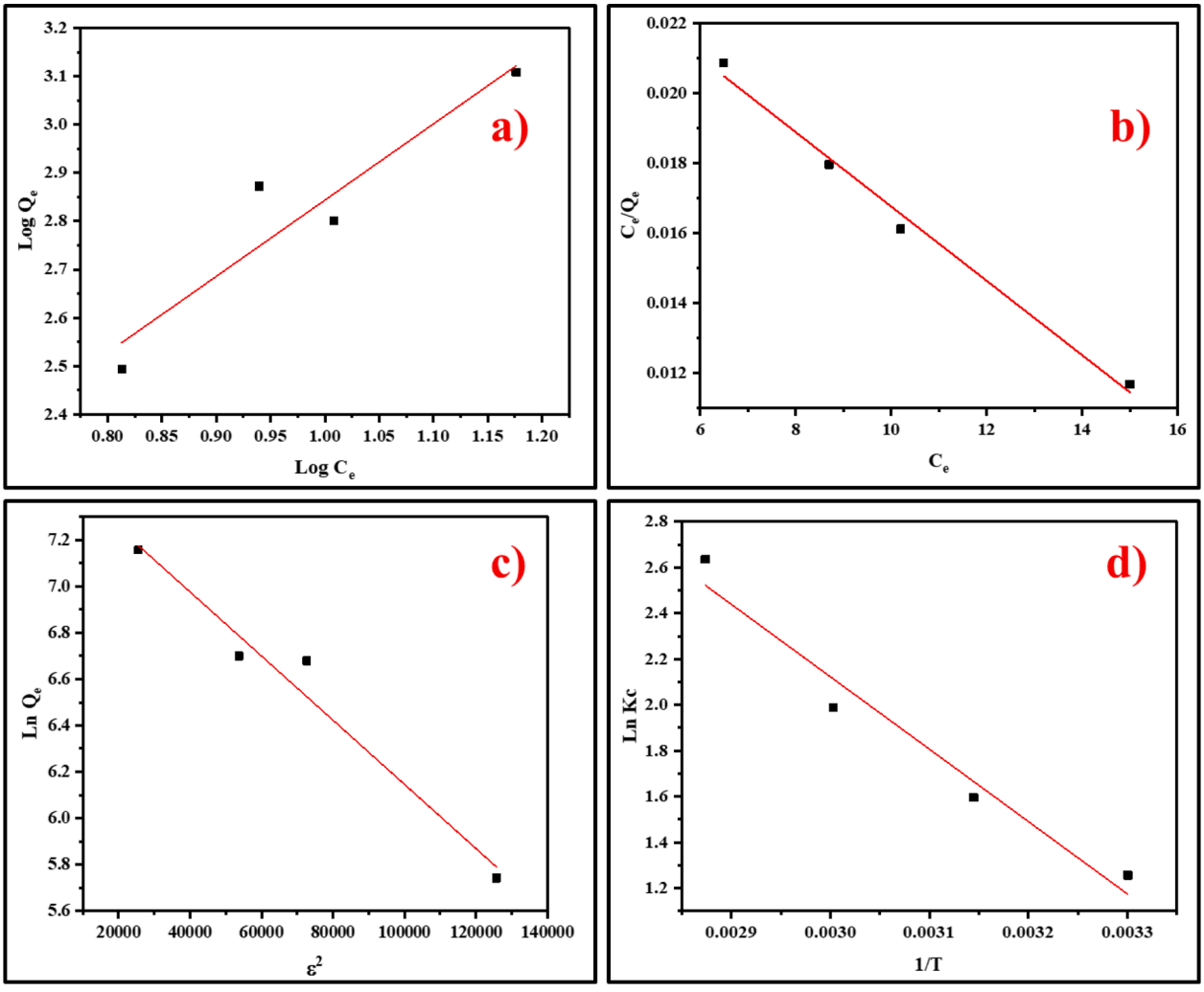

Fig. 7. a) Freundlich, b) Langmuir, c) D-R isotherm model for the adsorption (pH=6, Concentration=200 ppm, Dosage=20 g/L) and d) Thermodynamic parameters (pH=6, Concentration=200 ppm, Dosage=20 g/L, T = 303 K-348 K).

Table 4
Thermodynamics parameters of adsorption of Pb^{2+} (pH=7, Concentration=200 ppm, Dosage=20 g/L, T = 303 K-348 K).

Adsorbent	Temperature, K	R^2	ΔG^0 kJ/mol	ΔH^0 kJ/mol	ΔS^0 kJ/mol K
Pb^{2+}	303	0.98	−3.16	−26.27	0.096
	318		−4.21		
	333		−5.50		
	348		−7.62		

Table 5
BBD matrix of variables along with actual, fits, and residual values.

Trial No.	A	B	C	Pb^{2+} on TBBT-COF		
				Experimental value	Predicted value	Residual Removal
1	1	0	−1	97.1	92.9	3.14
2	1	−1	0	85.1	88.7	−2.63
3	0	−1	−1	53.9	54.4	−0.5
4	1	0	1	98.7	97.8	−0.68
5	−1	1	0	43.2	39.5	2.64
6	0	0	0	77.1	77.1	0
7	1	1	0	98.9	99.1	0.19
8	−1	0	1	24.2	28.3	−3.13
9	−1	0	−1	29.1	28.6	0.69
10	0	0	0	77.1	77.1	0
11	0	1	−1	69.1	73.1	−3.32
12	0	−1	1	61.7	57.6	3.33
13	0	1	1	76.2	75.7	0.5
14	0	0	0	77.1	77.1	0
15	−1	−1	0	13.2	13.1	−0.18

(R^2 = 0.94). This shows that a single layer of adsorbent has been observed on the surface of TBBT-COF and that once the surface is fully coated, no more adsorption will take place. Additionally, it was discovered that the separation factor (RL) value was 0.1 (0 RL 1), representing that the adsorption method in our situation is advantageous ($0<R_L<1$). The distribution of Gaussian energy over the uneven surfaces was evaluated using the Dubinin-Radushkevich isotherm [68]. The E value determines the type of adsorption: if $1<E<8$ kJ/mol, (physical phenomena); if $1<E<16$ kJ/mol, (ion exchange phenomena); and if $E>16$ kJ/mol, (chemical adsorption). The E values greater than 50 kJ/mol in the present study show the predominant chemical adsorption over the other two. It is clear from Table 3 that TBBT-COF has the highest or most equivalent adsorption capability of other inexpensive adsorbent materials.

By using van't Hoff law, the thermodynamic parameters are calculated.

$$\ln\left(k_c^0\right) = \frac{\Delta S^0}{R} - \frac{\Delta H^0}{RT}$$

where R; ideal gas constant (8.314 J/K.mol), T; is the temperature (K) and the equilibrium constant (Kc) was expressed as: Kd = Qe/Ce [69, 70]. Table 4 contains the values for the necessary thermodynamic parameters, and Fig. 7d depicts the van't Hoff equation for the adsorption of Pb^{2+} on the TBBT-COF surface. The fact that the free energies are negative for the temperature range under consideration shows that Pb^{2+} was successfully and quickly adsorbed on the TBBT-COF surface. The decreased ΔG^0 values with the increase in the temperatures (from 303 to 348 K) indicates the spontaneous sorption Pb^{2+} on TBBt-COF. The exothermic nature of Pb^{2+} sorption is concluded on the basis of negative ΔH^0 values with rising temperatures. Positive results of ΔS^0 indicated that there was greater randomness at the TBBT-COF contact throughout the adsorption process.

Table 6
Results of the ANOVA for the obtained quadratic equation of TBBT-COF.

Source	Sum of squares	Pb^{2+} on TBBT-COF		
		F-value	p-value	Significance
Model	10,449.81	61.75	0.00013	Significant
A-Time	9119.20	485.02	0.0019	Significant
B-pH	675.24	35.91	0.0018	Significant
C-Metal Concentration	16.82	0.89	0.387	
AB	65.61	3.489	0.1207	
AC	10.56	0.561	0.487	
BC	0.12	0.0065	0.938	
A^2	367.39	19.54	0.0068	Significant
B^2	182.22	9.691	0.026	Significant
C^2	86.85	4.619	0.084	

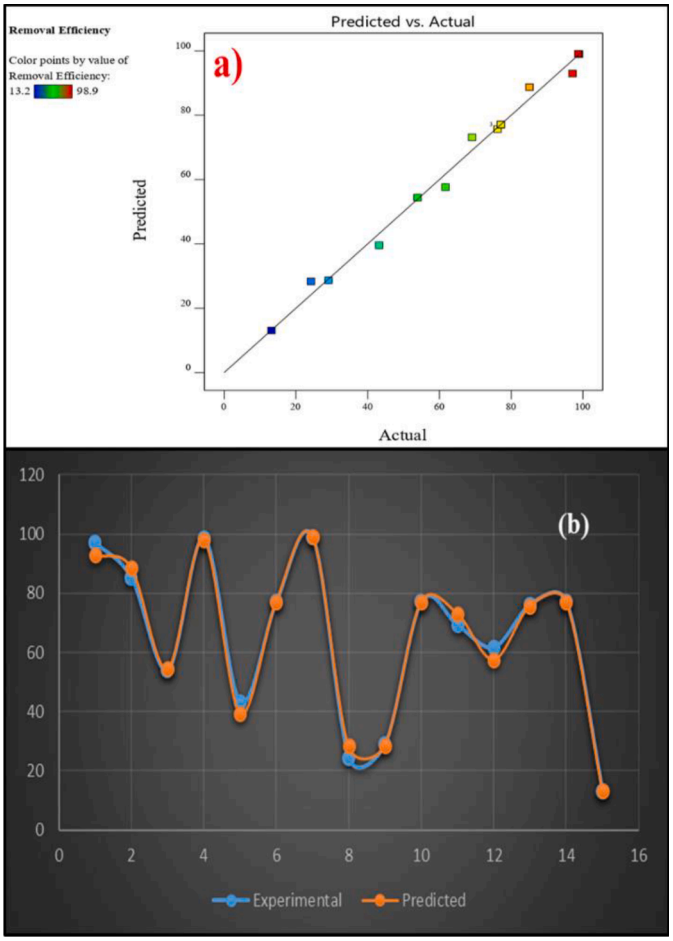

Fig. 8. a) Linear and (b) Non-Linear correlation between experimental and predicted Removal efficiency%.

3.4. Optimization of Pb^{2+} removal by TBBT-COF

As explained before, RSM was employed to evaluate the optimization and correlation of experimental factors. Table 5 comprises the BBD design matrix, accompanied by experimental and projected values. The considered response is theamount of metal ion adsorbed per unit mass of the adsorbent (mg/g) and the statistical relationship between the variables and the response is written as, $Y_{TBBT-COF}$, with coded values (A, B, and C) as shown in the equation below:

$$Y_{COF} = 77.1 + 33.7625 * A + 9.1875 * B + 1.45 * C - 4.05 * AB + 1.625 * AC - 0.175 * BC - 9.975 * A^2 - 7.025 * B^2 - 4.85 * C^2$$

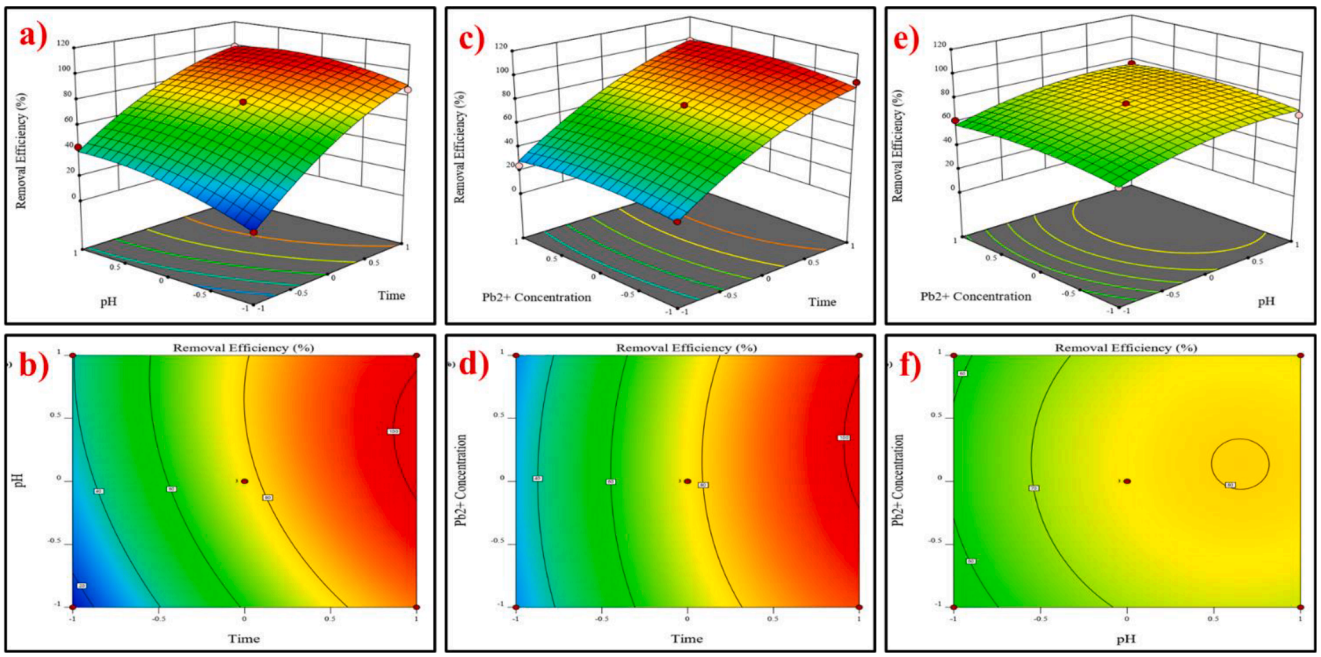

Fig. 9. The cumulative impact of pH, time and metal concentration (a), (c), (e) and 3D surface and (b), (d), (f) contour plots.

ANOVA of the regression model was used to establish the relevance of the primary influencing variables on the adsorption process.The ANOVA outcomes for the TBBT-COF quadratic equation are displayed in Table 6. The results of ANOVA show the appropriate relationship between the response and the contributing variables and found that well suitability of Pb^{2+} with the quadratic model. A smaller p value and a greater F value indicates that the regression equation will illustrate the key factors in the response. The model found to be statistically significant due to lower p values (less than 0.05). The large F value (61.76) for TBBT-COF could happen owing to noise in 0.01 percent of cases. From equation Y_{COF} The model parameters of Y_{COF}, i.e. A, B, A^2, B^2, are the model terms that are regarded as being important for response. The results were examined using the (R^2), and found to be in fair agreement as observed by R^2 of 0.857 (predicted) and 0.975 (adjusted). Fig. 8a and b displays the linear and non-linear relation between the experimental and predicted% removal. The graph shows the even distribution of the data points along a straight line in the linear graph, which had 0.99 R^2 value. The non-linear graph shows the close relationship between experimental and predicted values. The results further show that the quadratic model chosen is appropriate for Pb^{2+} elimination.

In order to further support the efficacy of these techniques, their effectiveness is statistically assessed using well-known statistical metrics. However, it does not accurately capture nonlinear relationships or error distribution. This method explains the magnitude and direction of linear relationships between experimental and model predictions. The experimental data and predictions have R^2 values of 0.99, which indicates that the suggested models closely match the experimental data. The APE was estimated to be 25.79 while the ARE was calculated to be 5.1589. The error deviation is noticeably less than what RSM projected, according to the estimated RMSE of 2.61. Additional metrics the Pearson's Chi-square measure offers a practical scale for measuring the goodness of fit, and it is determined to be 1.81 for RSM. HYBRID and MPSD are also significant for RSM.

3.4.1. Three-Dimensional response surface and two-dimensional contour plot

Both 2D contour plots and 3D response surface plots were used to assess the individual and relative effects of these variables on the response and to determine the ideal value. Each processing variable, including time, Pb^{2+} concentration and pH, affects TBBT-COF capacity for adsorption in a distinct way. Fig. 8a–f contains 3D surface and contour plots that illustrate the relative effects of time, pH, and Pb^{2+} concentration on the removal%.

Fig. 9a and b depicts the collective effect of pH and time on Pb^{2+} removal by TBBT-COF while keeping the Pb^{2+} concentration at zero (200 ppm). It was clear that increasing pH would aid in the elimination of Pb^{2+}. The maximum Pb^{2+} removal was observed between pH 6 and 8 in both the cases. The Pb^{2+} removal yield is more strongly prejudiced by the pH of the solution. This is most likely because a higher pH causes an increase in negatively charged binding sites, which may subsequently promote the adsorption of Pb^{2+} through electrostatic interactions. Additionally, it was interesting to notice that as adsorbate dosage is increased, Pb^{2+} removal efficiency improves. This pattern is explained by the fact that when the TBBT-COF dose increased, there were more active sites available. As the contact time between the adsorbent surface and the adsorbate was prolonged from 30 to 90 min, the removal effectiveness rose. A diagonally elongated homogeneous pattern could be seen in the contour plot that followed the TBBT-COF response surface plot, demonstrating that the interaction between pH and time had a major impact on Pb^{2+} removal.

Fig. 9c and d show the cumulative effect of time and Pb^{2+} concentration on Pb^{2+} elimination when the pH is set to zero (pH = 6.0). It was clear that when Pb^{2+} concentration grew from 100 to 300 ppm, the removal efficiency (Y) increased with little variation, reached its maximum value, and was heavily influenced by the contact time. The removal efficiency increased as the contact time between the adsorbent surface and the adsorbate was increased from 60 to 90 min. The response surface plot's conspicuous peak and the contour plot's elongated pattern demonstrate the significant mutual interaction between Pb^{2+} concentration and time.

Fig. 9e and f showed how the pH and Pb^{2+} concentration interacted while the time was zero (time 60 min). Increase in the pH and Pb^{2+} concentration result in enhanced Pb^{2+} removal capacity. However, pH 4 will achieve the removal of about 45 %. The greater elimination% is apparent between pH 6 and 8. When both variables are raised over a lengthy period of time, Pb^{2+} removal performance suffers. This is most likely brought on by a lack of readily available binding sites. The response surface plot revealed elevated graph for both the adsorbent

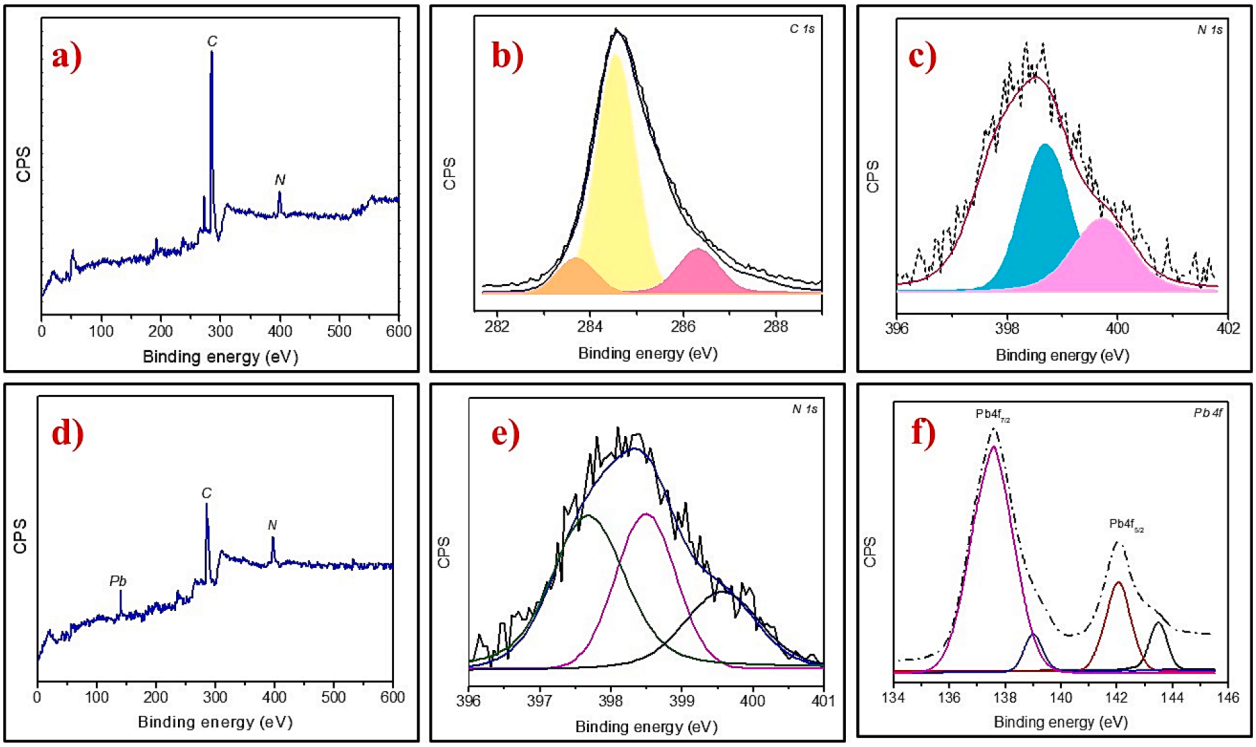

Fig. 10. XPS of TBBT-COF a-c) before adsorption and d-f) after adsorption of Pb^{2+}.

while the contour plot displayed a distinctive green coloured elongated pattern, showing that the interaction between Pb^{2+} concentration and pH had a substantial impact on Pb^{2+} removal.

Any approach that solicits a large number of replies and aims to analyse pertinent factors simultaneously employs optimisation. We selected time, pH, and Pb^{2+} concentration as the limits for the greatest response. Under the constraints, 200 ppm concentration at pH 6 and a 90 min contact duration are the ideal conditions for Pb^{2+} removal, with a response of 98.9 % by TBBT-COF.

3.4.2. *Stability and probable adsorption mechanism*

The stability and adsorption mechanism of the TBBT-COF were tried to be explored by a series of experiments along with advanced characterization techniques. Initially, TBBT-COF was dissolved in various organic solvents like methanol, ethyl acetate, DMF, hexane, THF, etc., and in almost all the solvents, the material was highly stable even after 12 h. In addition, TBBT-COF was dissolved even in boiling water, aqueous HCl, pH maintained at 2, and NaOH pH maintained at 10. In all the above harsh conditions, the material was found to be stable up to 92 %. Further, TBBT-COF was subjected to XRD, SEM and XPS before and after the adsorption process to understand the mechanism of adsorption and the morphological changes of TBBT-COF. XRD pattern Fig. S2 clearly shows that almost all the peaks of TBBT-COF are retained, but there is the appearance of new peaks at 37.72, 46.26, and 68.66 after the adsorption studies. This implies that the metal is accumulated on the surface of TBBT-COF. The Pb^{2+}ions cover the adsorbent's surface in the SEM image of the TBBT-COF after adsorption. Fig. S3 suggests the formation of a monolayer of the adsorbate molecule over the adsorbent's surface. Studies using scanning electron microscopy (SEM) visualised the growth of a molecular cloud of metal ions on the surface.

XPS studies were done on the samples to back up the data from EDS analysis and to look at the chemical make-up of the TBBT-COF before and after adsorption. The survey spectrum shows the presence of C 1 s, N 1 s in the sample before the adsorption. The deconvoluted spectra of carbon show a prominent peak at 286.36, 284.55, and 283.71 eV which correspond to the C—N, C—C, and C = C respectively. Similarly, the N 1 s spectrum shows the peak at 399.71 and 398.70 eV these are the characteristics of C—N and C = N and further confirm that imine linkage can be formed, which can create defects and active sites for the adsorption (Fig. 10a–c). The survey spectra of TBBT-COF after adsorption clearly show the presence of Pb. The peaks of C 1 s have been retained as such, but there are slight changes in the deconvoluted peak of N 1 s, including the appearance of a new peak in the range of 397.68 eV, which indicates the interaction of the metal ion with the imine bonds. All the above evidence clearly shows that TBBT-COF can be effectively used as an adsorbent (Fig. 10d-f).

3.4.3. *Real samples analysis*

Real waste water samples were taken from the Vrishabhavathi river near the Kengeri industrial sector of Bangalore for this study. Table S3 presents thorough analyses for the sample. The samples were therefore spiked with 0.5 mg/L of Cu (II), Pb (II), Cd (II), and Hg (I) to test the effectiveness of the TBBT-COF for the removal of heavy metals from real water samples. The original sample (non-spiked) had low levels of Cu (II), Cd(II), and Hg(I) removed, i.e., 68, 92, 73, and 76 %, respectively. The unusually high levels of the cations Na^{+}, K^{+}, Mg^{2+}, and Ca^{2+} in the waste water may be responsible for this effect. When cations are present in very high concentrations, they compete for the active sites of the TBBT-COF, which reduces the adsorption of heavy metals. The electrostatic attraction between the TBBT-COF surface and the heavy metal ions is also reduced by the positive layer of ions that forms around the TBBT-COFs. It is evident that the majority of the metal ions in the spiked sample were removed from the solution. Using TBBT-COF (300 ppm), Cu (II), Pb(II), Cd(II), and Hg(I) were each eliminated to a respective percentage of 77, 99, 82 and 83 %. The efficiency of removal by TBBT-COFs was found to be higher in the case of the spiked samples when compared to the original sample. This might be explained by the fact that, in comparison to the spiked samples, the original sample comprised excessive amounts of Na^{+}, K^{+}, Mg^{2+}, and Ca^{2+}. TBBT-COF is a multifunctional adsorbent which consists of imine linked nitrogen atoms and hexagonal conjugation rings. Nitrogen atoms have non-bonding electron pairs which can bind with analytes. Rings in its structure can conjugate

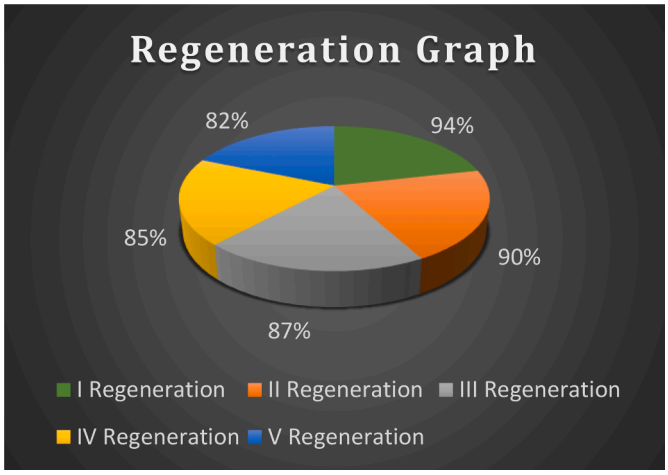

Fig. 11. Regeneration studies (pH=6, Concentration=200 ppm, Dosage=20 g/L).

Table 7
Comparison of adsorption capacity of Pb^{2+} using TBBT—COF with reported materials.

Sl. No.	Adsorbents	Adsorption capacity, (mg/g)	Reference
1	Ca-Fe/LDH—Cit	61.73	[71]
2	COOH@COF	123.8	[72]
3	N-CPF	816.0	[73]
4	UIO-66-TETA	641.03	[74]
5	DHTP-TPB COF	154.3	[75]
6	Ni0.6Fe2.4O4-HT-COF	411.80	[76]
7	DAA-TFPT-COF	128	[77]
8	ZIF-67/LDH@C	662.25	[78]
9	**TBBT-COF**	**601.6**	**Present Work**

and make π-π interactions with analytes. That means only the exposed imine groups are the effective and available sites for Pb^{2+} binding mainly via electrostatic attraction or complexation, while the stacking TBBT-COF sheets with intercalation and exfoliation will results in the adsorption of Pb^{2+}, which can further improve the adsorption capacity of these imine based TBBT-COF for heavy metal removal.

3.4.4. Regeneration capacity

For applications, it is important to conduct an analysis of regeneration capability. In this instance, the solvent regeneration technique has been used to recycle the adsorbent due to its ease of use, high efficacy, and low cost. Typically, the adsorbent is recycled in a 0.5 M HCl solution after being desorbed in a 0.5 M NaOH solution. As illustrated in Fig. 11, it was revealed that after five cycles, about 82 % of the Pb^{2+} removal effectiveness could be retained. This suggests using TBBT-COF as a sustainable adsorbent to remove metal ions from wastewater. The stability and absorption capacity of TBBT-COF towards adsorptive removal of Pb^{2+} is very good and comparable with many reported methods as shown in Table 7 [71–78].

4. Conclusions

Covalent organic frameworks have been synthesized using 3,3′,5,5′-tetramethyl-[1,1′-biphenyl] 4,4′-diamine and benzene-1,3,5-tricarbaldehyde through imine linkage via a solvothermal approach. The synthesized TBBT-COF has been used as an adsorbent for the removal of lead from waste water and has achieved 99 % removal. The PZC value of TBBT-COF was found to be 5.2. The maximum removal of $Pb^{2+}$was observed when the initial concentration of Pb^{2+}taken was 200 ppm . The reaction medium was found to favourable in acidic pH (6) compared to alkaline.The chemisorption of Pb^{2+}over the TBBT-COF was well supported by kinetic and isotherm models. The imine linkage helped ensure the strong and efficient binding of Pb^{2+} ions. The post-adsorption structural, morphological, and spectroscopic studies reveal the effective binding and removal of Pb^{2+}. The simulated adsorption studies were well correlated with the experimental results. The efficient removal of Pb^{2+}on TBBT-COF could be attributed to porosity, surface area, and covalent bonding. The present work could create a way for efficient removal of pollutants from water and further studies on increasing the efficiency of COFs.

Declaration of Competing Interest

The authors declare that they have no known competing financial interests or personal relationships that could have appeared to influence the work reported in this paper.

Data availability

Data will be made available on request.

Acknowledgments

The authors are immensely elated and wish to express their indebted gratitude to the Management of the Faculty of Engineering and Technology, Jain University and NHCE for providing lab facilities. Dr. Yogesh Kumar K thank Vision group on Science and Technology (VGST, GOK, India) for funding this project-GRD-959. Authors extend their thanks and appreciation to Research Supporting Project (RSP2024R160) King Saud University, Riyadh, Saudi Arabia. This work was funded by the Korea Institute of Energy Technology Evaluation and Planning (KETEP) of the Republic of Korea (RS-2023-00255939).

Supplementary materials

Supplementary material associated with this article can be found, in the online version, at doi:10.1016/j.apsadv.2023.100502.

References

[1] R. Szostak, Role of transportation in the industrial revolution a comparison of England and France, McGill-Queen's Press – MQUP. (1991) 1–334.
[2] E. Dana, Adsorption of heavy metals on functionalized-mesoporous silica a review, Microporous Mesoporous Mater. 247 (2017) 145–157.
[3] R.K. Sharma, M. Agrawal, F. Marshall, Heavy metal contamination of soil and vegetables in suburban areas of Varanasi, India, Ecotoxicol. Environ. Saf. 66 (2007) 258–266.
[4] J.G. Paithankar, S. Saini, S. Dwivedi, A. Sharma, D.K. Chowdhuri, Heavy metal associated health hazards an interplay of oxidative stress and signal transduction, Chemosphere 262 (2021) 128350–128365.
[5] W. Albouchi, M. Meftah, A.B.H. Amara, W. Oueslati, Effect of reactant ratio and nanofillers type on the microstructural properties, porosity fluctuations and heavy metal removal ability of chitosan-clay hybrid materials, Appl. Surf. Sci. Adv. 13 (2023), 100387.
[6] C.R. Manjunatha, B.M. Nagabhushana, M.S. Raghu, S. Pratibha, Perovskite lanthanum aluminate nanoparticles applications in antimicrobial activity, adsorptive removal of Direct Blue 53 dye and fluoride, Mater. Sci. Eng. C 101 (2019) 674–685.
[7] P.K. Asha, K. Deepak, M.K. Prashanth, L. Parashuram, V.S. Anusuya Devi, S. Archana, H. Shanavaz, S. Shashidhar, K.N. Prashanth, K. Yogesh Kumar, M. S. Raghu, Ag decorated Zn-Al layered double hydroxide for adsorptive removal of heavy metals and antimicrobial activity: numerical investigations, statistical analysis and kinetic studies, Environ. Nanotechnol. Monit. Manag. 20 (2023) 100787–100802.
[8] D. Vilela, J. Parmar, Y. Zeng, Y. Zhao, S. Sanchez, Graphene-based microbots for toxic heavy metal removal and recovery from water, Nano Lett. 16 (4) (2016) 2860–2866.
[9] C.V. Tran, D.V. Quang, H.P. Nguyen Thi, T.N. Truong, D.D. La, Effective removal of Pb (II) from aqueous media by a new design of Cu–Mg binary ferrite, ACS Omega, 5 (2020) 7298–7306.
[10] S.D. Faust, O.M. Aly, Chemistry of Water Treatment, 2nd ed., CRC Press, Chelsea, MI, 1998.
[11] World Health Organization, S. Water, H. Team, Guidelines for drinking-water quality in Recommendations 1 (2004).

[12] A.A. Hegazy, M.M. Zaher, M.A. Abd el hafez, A.A. Morsy, R.A. Saleh, Relation between anemia and blood levels of lead, copper, zinc and iron among children, BMC Res. Notes 133 (3) (2010) 1–9.

[13] L. Shvachiy, V. Geraldes, A. Amaro-Leal, I. Rocha, Intermittent low-level lead exposure provokes anxiety, hypertension, autonomic dysfunction and neuro inflammation, Neurotoxicology 69 (2018) 307–319.

[14] A.R. Abelsohn, M. Sanborn, Lead and children, Clin. Manag. Fam. Phys. 56 (2010) 531–535.

[15] F. Soori, A.N. Ejhieh, Synergistic effects of copper oxide-zeolite nanoparticles composite on photocatalytic degradation of 2,6-dimethylphenol aqueous solution, J. Mol. Liq. 255 (2018) 250–256.

[16] H. Hajjaoui, A. Soufi, M. Abdennouri, S. Qourzal, H. Tounsadi, N. Barka, Removal of cadmium ions by magnesium phosphate Kinetics, isotherm, and mechanism studies, Appl. Surf. Sci. Adv. 9 (2022) 100263–100272.

[17] H. Ozaki, K. Sharma, W. Saktaywin, Performance of an ultra-low-pressure reverse osmosis membrane (ULPROM) for separating heavy metal effects of interference parameters, Desalination 144 (1–3) (2002) 287–294.

[18] G. Al-Enezi, M.F. Hamoda, N. Fawzi, Ion exchange extraction of heavy metals from wastewater sludges, J. Environ. Sci. Health 39 (2004) 455–464.

[19] M.S. Raghu, K. Yogesh Kumar, M.K. Prashanth, B.P. Prasanna, Raj Vinuth, C. B. Pradeep Kumar, Adsorption and antimicrobial studies of chemically bonded magneticgraphene oxide-Fe_3O_4 nanocomposite for water purification, J. Water Process. Eng. 17 (2017) 22–31.

[20] C.R. Manjunatha, B.M. Nagabhushana, Anjana Naryana, P. Usha, M.S. Raghu, J. R. Adrsha, Adsorption of fluoride and DB-53 dye onto PLA/rGO nanoparticles: mathematical modeling and statistical studies, J. Water Process. Eng. 44 (2021) 102447–102460.

[21] H. Alrobei, M.K. Prashanth, C.R. Manjunatha, C.B. Pradeep Kumar, C. P. Chitrabanu, D.S. Prasanna, K. Yogesh Kumar, M.S. Raghu, Adsorption of anionic dye on eco-friendly synthesised reduced graphene oxide anchored with lanthanum aluminate: isotherms, kinetics and statistical error analysis, Ceram. Int. 47 (2021) 10322–10331.

[22] C.J. Madadrang, H.Y. Kim, G. Gao, N. Wang, J. Zhu, H. Feng, M. Gorring, M. L. Kasner, S. Hou, Adsorption behavior of EDTA-graphene oxide for Pb (II) removal, ACS Appl. Mater. Interfaces 4 (2012) 1186–1193.

[23] M.S. Raghu, K. Yogesh Kumar, Srilatha Rao, T. Aravinda, M.K. Prashanth, S. C. Sharma, Simple fabrication of reduced graphene oxide few layer MoS_2 nanocomposite for enhanced electrochemical performance in supercapacitors and water purification, Phys. B 537 (2018) 336–345.

[24] C.R. Manjunatha, B.M. Nagabhushana, A. Narayana, S. Pratibha, M.S. Raghu, Effective and fast adsorptive removal of fluoride on $CaAl_2O_4$: ba nanoparticles: isotherm, kinetics and reusability studies, Mater.Res. Express 6 (2019) 115089–115107.

[25] J. Zha, Y. Huang, W. Xia, Z. Xia, C. Liu, L. Dong, L. Liu, Effect of mineral reaction between calcium and aluminosilicate on heavy metal behavior during sludge incineration, Fuel 229 (2018) 241–247.

[26] M.K. Uddin, A review on the adsorption of heavy metals by clay minerals, with special focus on the past decade, Chem. Eng. J. 308 (2017) 438–462.

[27] G. Zhao, X. Huang, Z. Tang, Q. Huang, F. Niu, X. Wang, Polymer-based nanocomposites for heavy metal ions removal from aqueous solution: a review, Polym. Chem. 9 (2018), 3562–3582.

[28] A. Nayak, B. Bhushan, V. Gupta, P. Sharma, chemically activated carbon from lignocellulosic wastes for heavy metal wastewater remediation: effect of activation conditions, J. Colloid Interface Sci. 493 (2017) 228–240.

[29] L.P. Lingamdinne, Y.Y. Chang, J.K. Yang, J. Singh, E.H. Choi, M. Shiratani, J. R. Koduru, P. Attri, Biogenic reductive preparation of magnetic inverse spinel iron oxide nanoparticles for the adsorption removal of heavy metals, Chem. Eng. J. 307 (2017) 74–84.

[30] M. Dinari, S. Neamati, Surface modified layered double hydroxide/polyaniline nanocomposites synthesis, characterization and Pb^{2+} removal, Colloids Surf. A 589 (2020) 124438–124448.

[31] T. Salehi, M. Shirvani, M. Dinari, E. Gavili, Adsorptive removal of lead from water using a novel cysteine-bentonite/poly(vinyl alcohol)/alginate nanocomposite, J. Polym. Environ. 30 (2022) 4463–4478.

[32] F. Parsadoust, M. Shirvani, H. Shariatmadari, M. Dinari, Kinetics of lead remobilization from montmorillonite by glutamate diacetate (GLDA), methylglycine diacetate (MGDA), and ethylenediamine tetraacetate (ETDA) chelating agents, Environ. Process. 9 (2022) 41.

[33] M. Aghaei, A.H. Kianfar, M. Dinari, Synthesis and characterization of a novel Schiff base polyamide ligand and its copper(II) complex for comparative removal of Pb (II) ions from aqueous solutions, J. Polym. Res. 27 (2020) 54.

[34] M. Dinari, A. Haghighi, Efficient removal of hexavalent chromium and lead from aqueous solutions by s-triazine containing nanoporous polyamide, Polym. Adv. Technol. 28 (2017) 1683–1689.

[35] R. Zhu, J. Ding, L. Jin, H. Pang, Interpenetrated structures appeared in supramolecular cages, MOFs, COFs, Coord. Chem. Rev. 389 (2019) 119–140.

[36] Y. Peng, H. Huang, Y. Zhang, C. Kang, S. Chen, L. Song, D. Liu, C. Zhong, A versatile MOF-based trap for heavy metal ion capture and dispersion, Nat. Commun. 9 (2018) 1–9.

[37] H. Shanavaz, N. Kannanugu, D. Kasai, K. Yogesh Kumar, M.S. Raghu, M. K. Prashanth, B.H.Jeon M.A. Khan, E. Linul, Covalent organic frameworks as promising materials: review on synthetic strategies, topology and application towards supercapacitors, J. Energy Storage 71 (2023), 108006.

[38] A.T. Partho, M. Tahir, B. Tahir, Recent advances in covalent organic framework (COF) nanotextures with band engineering for stimulating solar hydrogen production: a comprehensive review, Int. J. Hydrogen Energy 47 (2022) 34323–34375.

[39] A. Padamurthy, J. Nandanavanam, P. Rajagopalan, Preparation and characterization of metal organic framework based composite materials for thermochemical energy storage applications, Appl. Surf. Sci. Adv. 11 (2022) 100309–100320.

[40] F. Jiang, Y. Wang, T. Qiu, G. Yang, C. Yang, J. Huang, Z. Fang, J. Li, Synthesis of biphenyl-linked covalent triazine frameworks with excellent lithium storage performance as anode in lithium ion battery, J. Power Sources 523 (2023) 231041–231050.

[41] N.A. Rejali, M. Dinari, Y. Wang, Post-synthetic modifications of covalent organic frameworks (COFs) for diverse applications, ChemComm 59 (2023) 11631–11647.

[42] H. Shanavaz, B.P. Prasanna S. Archana M.K. Prashanth, M.S. Raghu R. Zhou, F. A. Alharthi B.H. Jeon, K. Yogesh Kumar, Niobium doped triazine based covalent organic frameworks for supercapacitor applications, J. Energy Storage 67 (2023) 107561–107574.

[43] R. Kamai, K. Kamiya, K. Hashimoto, S. Nakanishi, Oxygen-tolerant electrodes with platinum-loaded covalent triazine frameworks for the hydrogen oxidation reaction, Angew. Chem. 55 (2016) 13184–13188.

[44] C. Zhanga, M. Cuia, J. Rena, Y. Xinga, N. Lia, H. Zhaoa, P. Liua, X. Jib, M. Lib, Facile synthesis of novel spherical covalent organic frameworks integrated with Pt nanoparticles and multiwalled carbon nanotubes as electrochemical probe for tanshinol drug detection, Chem. Eng. J. 401 (2020) 126025–126035.

[45] X. Li, C. Yang, B. Sun, S. Cai, Z. Chen, Y. Lv, J. Zhang, Y. Liu, Expeditious synthesis of covalent organic frameworks: a review, J. Mater. Chem. A 8 (2020) 16045–16060.

[46] M. Zhang, J. Chen, S. Zhang, X. Zhou, L. He, M.V. Sheridan, M. Yuan, M. Zhang, L. Chen, X. Dai, Electron beam irradiation as a general approach for the rapid synthesis of covalent organic frameworks under ambient conditions, J. Am.Chem. Soc. 142 (2020) 9169–9174.

[47] S.T. Emmerling, L.S. Germann, P.A. Julien, I. Moudrakovski, M. Etter, T. Friscic, R. E. Dinnebier, B.V. Lotsch, In situ monitoring of mechanochemical covalent organic framework formation reveals templating effect of liquid additive, Chem. 7 (2021) 1639–1652.

[48] S. Archana, B.K. Jayanna, A. Ananda, B.M. S, D. Pandiarajan, H.B. Muralidhara, K. Y. Kumar, Synthesis of nickel oxide grafted graphene oxide nanocomposites—a systematic research on chemisorption of heavy metal ions and its antibacterial activity, Environ. Nanotechnol. Monit. Manag. 16 (2021) 100486–100499.

[49] S. Archana, B.K. Jayanna, A. Ananda, M.S. Ananth, A. Mossad Ali, H. B. Muralidhara, K.Y. Kumar, Numerical investigations of response surface methodology for organic dye adsorption onto Mg-Al LDH -GO Nano Hybrid: an optimization, kinetics and isothermal studies, J. Ind. Chem. Soc. 99 (2022) 100249–100263.

[50] S. Lagergren, Zur Theorie der Sogenannten Adsorption Gelöster Stoffe, Kungliga Svenska Vetenskapsakademiens, (1898) 1–39.

[51] Y.S. Ho, G. McKay, Pseudo-second order model for sorption processes, Process Biochem. 34 (1999) 451–465.

[52] A. Pholosi, E.B. Naidoo, A.E. Ofomaja, Intraparticle diffusion of Cr(VI) through biomass and magnetite coated biomass: a comparative kinetic and diffusion study, S. Afr. J. Chem. Eng. 32 (2020) 39–55.

[53] C. Aharoni, F.C. Tompkins, Kinetics of adsorption and desorption and the elovich equation, Adv. Catal. 21 (1970) 1–49.

[54] I. Langmuir, The adsorption of gases on plane surfaces of glass,mica and platinum, J. Am.Chem. Soc. 60 (1918) 467–475.

[55] H. Freundlich, Colloid and Capillary Chemistry, Methuen, London, 1926, pp. 114–122.

[56] J.S. Piccin, G.L. Dotto, L.A.A. Pinto, Adsorption isotherms and thermochemical data of FD and C RED N° 40 Binding by chitosan, Braz. J. Chem. Eng. 28 (2011) 295–304.

[57] S. Parambadath, A. Mathew, S.S. Park, C.S. Ha, Pentane-1,2-dicarboxylic acid functionalized spherical MCM-41: a simple and highly selective heterogeneous ligand for the adsorption of Fe3+ from aqueous solutions, J. Environ. Chem. Eng. 3 (2015) 1918–1927.

[58] S. Parambadath, A. Mathew, M.J. Barnabas, S.Y. Kim, C.S. Ha, Concentration-dependant selective removal of Cr(III), Pb(II) and Zn(II) from aqueous mixtures using 5-methyl-2-thiophenecarboxaldehyde Schiff base-immobilised SBA-15, J. Solgel Sci. Technol. 79 (2016) 426–439.

[59] R.G. Pearson, Hard and soft acids and bases, HSAB, part 1: fundamental principles, J. Chem. Educ. 45 (1968), 581-587.

[60] Pearson | Hard | Soft | Acid | Base | Chemogenesis, (n.d.). https://www.meta-synthesis.com/webbook/43_hsab/HSAB.php (accessed June 29, 2023).

[61] M. Laing, The electronegativity of a metal and its E°: should they correlate? S. Afr. J. Sci. 98 (2002) 573–580.

[62] J. Di, Z. Ruan, S. Zhang, Y. Dong, S. Fu, H. Li, G. Jiang, Adsorption behaviors and mechanisms of Cu2+, Zn2+ and Pb2+ by magnetically modified lignite, Sci. Rep. 12 (2022) 1394.

[63] B.B. Mohammed, A. Hsini, Y. Abdellaoui, H.A. Oualid, M. Laabd, M.E. Ouardi, A. A. Addi, K. Yamni, N. Tijani, Fe-ZSM-5 zeolite for efficient removal of basic Fuchsin dye from aqueous solutions: synthesis, characterization and adsorption process optimization using BBD-RSM modeling, J. Environ. Chem. Eng. 8 (2020) 104419–104430.

[64] S. Archana, D. Radhika, B.K. Jayanna, K. Kannan, K. Yogesh Kumar, H. B. Muralidhara, Functionalization and partial grafting of the reduced graphene oxide with p-phenylenediamine: an adsorption and photodegradation studies, FlatChem 26 (2020) 100210–100221.

[65] Y.S. Ho, J.C.Y. Ng, G. McKay, Removal of Lead(Ii) from effluents by sorption on peat using second-order kinetics, Sep. Sci. Technol. 36 (2006) 241–261.
[66] M. Afshari, M. Dinari, K. Zargoosh, H. Moradi, Novel triazine-based covalent organic framework as a superadsorbent for the removal of Mercury(II) from aqueous solutions, Ind. Eng. Chem. Res. 59 (2020) 9116–9126.
[67] J. Di, Z. Ruan, S. Zhang, Y. Dong, S. Fu, H. Li, G. Jiang, Adsorption behaviors and mechanisms of Cu^{2+}, Zn^{2+} and Pb^{2+} by magnetically modified lignite, Sci. Rep. 12 (1394) (2022) 1–18.
[68] N.H. Yusof, K.Y. Foo, L.D. Wilson, B.H. Hameed, M.H. Hussin, S. Sabar, Microwave-assisted synthesis of polyethyleneimine grafted chitosan beads for the adsorption of acid red 27, J. Polym. Environ. 28 (2020) 542–552.
[69] A.K. Singh, R.K. Gautam, S. Agrahari, J. Prajapati, I. Tiwari, Graphene oxide supported Fe_3O_4-MnO_2 nanocomposites for adsorption and photocatalytic degradation of dyestuff: ultrasound effect, surfactants role and real sample analysis, Int. J. Environ. Anal. Chem. (2022), https://doi.org/10.1080/03067319.2022.2091930.
[70] X. Wang, Y. Pei, M. Lu, X. Lu, X. Du, highly efficient adsorption of heavy metals from wastewaters by graphene oxide-ordered mesoporous silica materials, Chem. Eng. J. Adv. 50 (2015) 2113–2121.
[71] O. Rahmanian, M. Dinari, S. Neamati, Synthesis and characterization of citrate intercalated layered double hydroxide as a green adsorbent for Ni^{2+} and Pb^{2+} removal, Environ. Sci. Pollut. Res. 25 (2018) 36267–36277.
[72] X.F. Lu, W.H. Ji, L. Yuan, S. Yu, D.S. Guo, Preparation of carboxy-functionalized covalent organic framework for efficient removal of Hg^{2+} and Pb^{2+} from water, Ind. Eng. Chem. Res. 58 (38) (2019) 17660–17667.
[73] L.L. Peng, W.F. Zhou, W.F. Xu, Y. Liu, C.S. Zhou, J. Xie, K.W. Tang, Nitrogen-rich covalent phosphazene-based framework for efficient removal of lead(ii) ions, New J. Chem. 47 (2023) 6095–6101.
[74] H. Zhao, J. Sun, Y. Du, M. Zhang, Z. Yang, J. Su, X. Peng, X. Liu, G. Sun, Y. Cui, Efficient and selective removal of Pb2+ from aqueous solutions by modified metal-organic frame materials, Microporous Mesoporous Mater. 359 (2023) 112632–112641.
[75] A.M. Elewa, A.F.M. El-Mahdy, H.H. Chou, Effective remediation of Pb^{2+} polluted environment by adsorption onto recyclable hydroxyl bearing covalent organic framework, Environ. Sci. Pollut. Res. 30 (2023) 32371–32382.
[76] S. Wang, H. Wang, S. Wang, L. Fu, L. Zhang, Novel magnetic covalent organic framework for the selective and effective removal of hazardous metal Pb(II) from solution: synthesis and adsorption characteristics, Sep. Purif. Technol. 307 (2023) 122783–122796.
[77] Q. Ma, X. Liu, J. Qian, Q. Zhuang, Preparation of covalent organic framework with carboxy and triazine for efficient removal of Pb^{2+} ions, Sep. Purif. Technol. 323 (2023) 124368–124378.
[78] H. Cai, K. Ma, Y. Zhang, X. Li, W. Wang, S. Tong, Carbonizing hollow metal–organic framework/layered double hydroxide (MOF/LDH) nanocomposite with excellent adsorption capacity for removal of Pb(II) and organic dyes from waste water, Carbon Res. 2 (2023) 1–18.